**TITLE**

# Long-Term Monolayer Cultivation Captures Homeostatic and Regenerative Features of Human Colonic Epithelial Cells

Satoru Fujii,[1,2] Yi Wang,[3] Shanshan Meng,[1] Ryan J. Musich,[1] Scott T. Espenschied,[1] Kevin Newhall,[1] Yi Han,[1] Shuhei Sekiguchi,[2] Ryoma Matsumoto,[2] Matthew A. Ciorba,[4] L. David Sibley,[5] Ryuichi Okamoto,[2] Thaddeus S. Stappenbeck[1,6,*]

[1]Department of inflammation and immunity, Learner Research Institute, Cleveland Clinic, Cleveland, OH 44195, USA

[2]Department of Gastroenterology and Hepatology, Tokyo Medical and Dental University, Tokyo 113-8510, Japan

[3]Department of Pathology and Immunology, Washington University School of Medicine, Saint Louis, MO 63110, USA

[4]Division of Gastroenterology and the Inflammatory Bowel Diseases Center, Department of Internal Medicine, Washington University School of Medicine, St. Louis, , MO 63110, USA

[5]Department of Molecular Microbiology, Washington University School of Medicine, St Louis, MO, 63110, USA.

[6]Lead contact

[*]Correspondence: stappet@ccf.org

**SUMMARY**

While organoid culture technique has significantly advanced research on intestinal epithelial cells (IECs), reproducing the homeostatic and regenerative processes of human IECs in vitro remains challenging. We previously established a unique long-term 2-dimensional (2D) cultivation for mouse IECs using the air-liquid interface (ALI) technique, successfully recapitulating homeostasis and regeneration. Here, applying this to human IECs, we developed a long-term, self-organizing 2D cultivation for human IECs. During the culture, we observed a dynamic transition in cellular shape from squamous to columnar, resembling in vivo regeneration. RNA sequencing indicated that intestinal stem cells (SCs) with canonical SC markers like LGR5 may play a main role in both homeostasis and regeneration. Moreover, we identified minor populations, including deep crypt secretory (DCS)-like cells, CA7-positive cells, and non-canonical Goblet cells, previously overlooked in vitro. This novel technique holds promise for not only broadening our understanding of homeostasis, regeneration, and the functions of minor populations as well as SCs in human intestinal mucosa, but also facilitating future studies such as analyzing host-microbe interactions.

## INTRODUCTION

The intestinal epithelium is a selectively permeable barrier which functions as the primary interface between the host and the milieu of microorganisms and nutrients which reside in or pass through the intestine. In mammals, the intestinal epithelium is comprised of a monolayer of polarized cells including SCs, transient-amplifying (TA) cells, absorptive enterocytes (ECs), goblet cells (GCs), enteroendocrine cells (EECs), and some minor populations such as Tuft cells (TCs), to execute multiple functions like digestion, absorption, and mucosal immunity.

3-dimensional (3D) culture methods using primary IECs from mice or human donors were reported from several groups a decade ago[1–4]. While they have made revolutionary contributions in advancing basic and clinical science in this field, several limitations remain to be overcome. For example, recreating the regenerative process of IECs in 3D culture is challenging due to difficulties in maintaining cell viability after injury.

We previously established a novel ALI cultivation method of mouse IECs which yielded self-organizing, long-term 2D cultures that could recapitulate homeostatic and regenerative processes of IECs[5]. This enabled us to analyze regenerative IECs transitioning from injury-like squamous to homeostasis-like columnar morphologies, and consequently identified Hopx$^{+}$ cells as colitis-associated regenerative stem cells (CARSCs)[5]. In our current study, we applied this technique to patient derived IECs for further understanding homeostasis and regeneration of human IECs from a new perspective.

## RESULTS

We applied our ALI culture technique to human colon epithelial cells derived from healthy donors. Briefly, dissociated human IECs prepared from 3D spheroids were seeded onto transwell membranes and submerged in L-WRN conditioned media with rock inhibitor (Y-27632) and TGF-beta inhibitor (SB 431542 or A83-01) for 5-7 days until confluency. Monolayers were subsequently exposed to air to establish ALI for up to 28 days. Like mouse cells, we observed a continuous 2D monolayer, but no crypt-like folding structures. The monolayer cells were squamous with no indication of cellular differentiation at ALI day 0 (ALId0), which was reminiscent of squamous epithelia commonly observed in the region of crypt abscess in ulcerative colitis (UC) patients (Figure S1A). They subsequently grew columnar which coincided with the emergence of GC-like and EC-like cells by ALId7, resembling the homeostatic cellular structure of human colon as ALI culture progressed (Figure 1A). The cell height plateaued around 40 $\mu$m (Figure 1B), which is comparable to IEC height observed in human colon tissue[6]. Of note, while TGF-beta inhibitors are essential for 3D human IEC culture[3], they were dispensable for the 2D monolayer cells. Additionally, these culture conditions were permissive for polarization and differentiation of IECs from the human small intestine[7] (Figure S1B).

Immunofluorescence staining revealed that cultures after ALId7 contained common differentiated cell types including SLC26A3-positive ECs, MUC2-positive GCs, and CHGA-positive EECs (Figure 1C), while none of these were observed in the squamous monolayer at ALId0. Moreover, the presence of an overlying mucus layer suggests GCs are functional in the system and may establish barrier properties sufficient

to protect cells from bacterial pathogens much like the mucosa *in vivo* (Figure S1C and S1D). Transmission electron microscopy (TEM) analysis revealed ultrastructural features of ECs, GCs, and EECs (Figure 1D). The columnar cells at ALId28 can be passaged to both 2D ALI monolayers and 3D spheroids, demonstrating the existence of SCs in the monolayer even after 1 month culture (Figure S1E). EdU incorporation assays revealed that the IEC monolayer was hypo-proliferative at ALId0, transiently became hyper-proliferative around ALId2-d4, followed by a gradual return to be less proliferative thereafter (Figure 1E, S1F).

Bulk mRNA sequencing (RNAseq) at multiple time points showed dynamic transitions in gene expression during the ALI culture (Figure 1F). Canonical SC markers (LGR5, OLFM4, ASCL2, SMOC2) and proliferation markers (MKI67, PCNA) peaked at ALId4, supporting the finding of the EdU analysis. This also suggests that SCs expressing the canonical markers, but not HOPX, mediate human IEC proliferation and differentiation. We also observed marked induction of transcription factors required for secretory differentiation (*ATOH1, SPDEF, NEUROG3*) at ALId4, preceding the emergence of GC and EEC markers. EC markers (CA1, CA4, SLC26A3) followed a similar pattern except for AQP8, a mature EC marker, which emerged at ALId7, suggesting that EC maturation may require a longer time compared to GCs and EECs under this condition. Quantitative PCR (qPCR) analysis of transcripts associated with SCs, proliferative, and differentiated cells with higher temporal resolution supported the bulk RNAseq findings (Figure 1I). Furthermore, gene set enrichment analysis (GSEA) revealed that genes related to mouse IEC regeneration after dextran sodium sulfate (DSS)-induced colitis were significantly enriched in the squamous cells at ALId0

compared to ALId7, which aligned with the trends observed in mouse ALI cells[5]. (Figure 1G). GSEA also indicated a significant correlation between a UC epithelial signature and the squamous cells at ALId0, and a healthy epithelial signature and the homeostatic columnar cells at ALId7 (Figure 1H). Since we previously proposed that mouse ALI cells contains features as follows; i) squamous cells at ALId0 mimic the characteristics of inflamed mucosa in DSS-induced colitis, ii) hyper-proliferative cells observed around ALId2-d4 replicate the regenerative mucosa recovering from injury, and iii) columnar monolayer cells observed after ALId7 resemble the homeostatic mucosa[5], the histological and transcriptional findings so far suggested that the human IEC ALI culture recapitulates the epithelial features of injury, regeneration, and homeostasis, as shown in the mouse model.

We and another group previously reported that regenerating IECs adopt a fetal-like expression profile, considered essential for inducing a regenerative program in mice IECs[8,5]. GSEA revealed an enrichment of fetal-like genes at ALId0 (Figure S1G), suggesting ALId0 cells have activated a regenerative program defined in part by expression of fetal-like genes. YAP signaling, considered crucial for SC expansion, regeneration, and induction of fetal-like genes, was assessed as well. GSEA showed a high enrichment of YAP target genes at ALId0 compared to ALId7 (Figure S1H). High expression of major YAP target genes at ALId0 and subsequent reduction were also observed (Figure S1I). These finding suggested that YAP signaling mainly functions in the survival of squamous IECs during the submerged culture period, rather than in SC expansion and regeneration. WNT signaling is another essential pathway for SC maintenance. Most canonical WNT target genes exhibited higher expression at ALId0

and ALId4 than at later time points, suggesting a role for WNT signaling in regulating IECs survival and expansion during the early phase of ALI culture (Figure S1J). Of note, since WNT ligands are uniformly supplemented in the ALI culture media, WNT signaling of each IEC should be regulated independently of exogenous WNT gradient. Collectively, these findings suggest that the signaling of fetal-like genes, YAP, and WNT is associated with the cellular response during injury and regeneration in human IECs.

To further dissect the transcriptomic heterogeneity of cultured human IECs, we performed single-cell RNA sequencing (scRNAseq) on three colon lines derived from healthy donors at ALId7, when cells have begun to differentiate and adopt a columnar morphology similar to what is observed in homeostasis. Uniform Manifold Approximation and Projection (UMAP) clustering, heatmap, and dot plot analyses on the integrated dataset from the three lines revealed eleven distinct clusters within the homeostatic columnar monolayer cells containing major lineages including SCs (Cluster #1), TA cells (#2), ECs (#3, #4), GCs (#5), and EECs (#10) (Figure 2A-C), while IEC 3D spheroids consisted of mostly a single large cluster (Figure S2A).

SCs, defined by canonical SC markers including OLFM4 and LGR5 as in bulk RNAseq, constituted a small cluster (#1) with differential expression of these genes (Figure 2D, 2F). LGR5, regarded as the most specific SC marker in both humans and mice, was distinctly expressed in this cluster, and RNAscope *in situ* hybridization confirmed its expression within the monolayer cells. (Figure 2E). Contrarily, HOPX expression was minimal across the clusters, and quiescent or reserve SC markers (LRIG1, BMI1), which were defined in mice, showed expression profiles unspecific to the SC cluster (Figure 2F, S2B). Considering these results along with the bulk RNAseq

findings, these non-canonical SC marker genes may not be relevant to SC functions in homeostasis or regeneration of human mucosa. Cell cycle analysis (Figure 2G) revealed that only 30% of SCs reside in S or G2M phase, which was consistent with previous scRNAseq studies on human IECs[9] and mouse xenograft models[10], suggesting slower cycling in human colonic SCs compared to mice. TA cells, identified by MKI67 and PCNA, exhibited a fast cell cycle with 90% of them residing in S or G2M phase (Figure 2G). PCNA-positive cells are mainly in S phase, whereas MKI67-positive cells are in G2M phase, indicating a possible subdivision of TA cells based on cell cycle differences. (Figure S2C-S2D).

We assigned GC population (#5) based on the expression of canonical GC markers such as MUC2, TFF3, and FCGBP. We also assigned two sub-clusters neighboring the GC cluster to GC-sub1 and GC-sub2. The overall expression profile of GC-sub1 cells closely resembles that of GCs, with somewhat higher mitochondrial gene ratio (Figure S2E), suggesting that GC-sub1 cells may represent a stressed or dying population of GCs. Conversely, distinct differences in gene expression were observed between GC-sub2 and the others, as GC-sub2 cells expressed specific genes like REG4 and AGR2 (Figure 2B-2C, S2K). These genes are reported as markers for DCS cells in mice[11–13], leading us to designate this as DCS-like cluster.

In addition to canonical GCs, recent studies indicated the presence of non-canonical GCs (nc-GCs), which show enriched expression not only of GC markers but also of EC-associated genes[14]. Examining the small cluster (#8) near the GC cluster (#5), we identified the co-expression of several EC markers including SLC26A3 along with GC markers in this cluster. Therefore, we assigned this to nc-GC cluster. Pathway analysis

of GC cluster genes revealed a biosynthesis signature of mucin type o-glycan, a major component of intestinal mucin (Figure 2H)[15]. In contrast, pathway analysis of nc-GC cluster genes indicates an association with mineral absorption, a major function of ECs (Figure 2I)[16]. These findings demonstrate distinctive functions between GCs and nc-GCs in the human mucosa. We specifically observed the expression of PLCG2 in this cluster (Figure 2B-2C, S2F), suggesting PLCG2 as a candidate marker for nc-GCs.

We previously reported BEST4-positive cells as a lineage of mature absorptive enterocytes in humans[17]. Intriguingly, cells in cluster #9 expressed distinctive genes including BES4, OTOP2, CA7, and NOTCH2, which were reported to be expressed in the BEST4-positive cells[18]. We observed more uniform expressions of CA7 than BEST4 in this cluster (Figure S2G), promoting us to assign this to CA7 cluster. RNAscope analysis detected a CA7-positive population in both ALI cells and human colonic tissues (Figure 2J), affirming the reliability of our scRNAseq analysis in identifying this minor population *in vitro*. We also verified the high expression of SPIB, a transcription factor crucial for M cell differentiation in mice[19], within this cluster (Figure S2H). Subsequent analysis uncovered the preferential expression of GP2, a recognized M cell marker and target gene of SPIB[19], in this cluster (Figure S2H). This observation lends support to the hypothesis that the SPIB expression may be associated with the induction of CA7-positive cells.

In human IECs, EECs consist of sub-populations that produce different types of hormones. Additional transcriptomic investigation into ECC cluster (#10) revealed presence of L-cells, expressing PYY and glucagon, enterochromaffin cells (ECs), expressing TPH1, and progenitor cells expressing NEUROG3 (Figure 2K, S2I-S2J).

Immunofluorescence of NEUROG3, Serotonin (EC marker), and GLP-1 (L-cell marker) in ALId7 cells corroborated this scRNAseq analysis (Figure 2L). Of note, a subset of EECs in ALId7 monolayer cells exhibits distinctive SST expression, indicating the presence of D-cells (Figure 2K-2L, S2I), which previous scRNAseq studies failed to identify in human colon tissue or organoids[18,20,21]. Consistently, this corroborates the notion that the ALI cultured cells faithfully replicate *in vivo* differentiation programs, yielding minor populations of the human colon.

In addition, we identified a small cluster (#11) with distinctive expression of TRPM5, a putative maker for Tuft cells (TCs). Consequently, we assigned this to Tuft cell cluster. Genes such as PTGS1, TAS1R3, and POU2F3, enriched in this cluster, can be promising markers for labeling TCs in human intestinal mucosa (Figure 2C).

In summary, human colonic monolayer cells at ALId7 recapitulated the homeostatic biology of human colonic epithelial mucosa. The observed transition from squamous cells at ALId0 to columnar cells at ALId7 will provide valuable insights into the cellular plasticity crucial for IEC regeneration after injury. Also, the homeostatic columnar ALI cells contain not only major populations, but also minor populations such as DCS-like cells, nc-GCs, CA7-positive cells, and D-cells. Thus, this ALI culture technique emerges as a fundamental tool for studying human mucosal physiology in homeostasis, regeneration mechanisms, and the pathophysiology of intestinal diseases including inflammatory bowel disease.

## DISCUSSION

We established a long-term, self-organizing monolayer culture for IECs

from human colon. We observed the dynamic transition in cellular shape from squamous at ALId0 to columnar at ALId7, which was reminiscent of IEC regenerative process recovering to homeostasis *in vivo*. Transcriptome analyses of human ALI cells suggest that cells expressing canonical SC markers, such as LGR5 and OLFM4, presumably play a key role in both homeostasis and regeneration in human IECs. This is in contrast to HOPX, which we previously identified using mouse ALI culture as a CARSC gene crucial for IEC regeneration in mice. While human IECs in ALI culture exhibited almost similar behavior to mouse cells, this different expression pattern of SC markers represented one of few discrepancies between human and mice ALI cells, underscoring a clear distinction in SC functions between the two.

GSEA analyses revealed fetal-like and YAP target genes were enriched in squamous cells at ALId0. YAP signaling is widely accepted to potentiate inductions of fetal-like genes and trigger a regeneration program in mice[8,22]. Our results supported the notion that the same phenomenon could be induced in the human colon. These signaling pathways may be crucial for inducing reprogramming necessary for the cellular shape transition to squamous during submerge culture, rather than for IEC expansion in the early stage of ALI culture. Focusing on WNT signaling, human IECs intriguingly appeared to possess an auto-regulation system for WNT signaling, as cellular responses transitioned during ALI culture despite the uniform supplementation of exogenous WNT ligands.

In addition to delineating the distinct separation of major IEC populations, scRNAseq analysis of the human homeostatic IECs monolayer unexpectedly detected several minor populations, some of which were not identified in previous reports. BEST4-

positive cells, which we previously reported as a sub-population of absorptive enterocytes in human colon epithelia[17], formed a definite population within the monolayer cells. Compared to BEST4, CA7 appears to be a more specific marker, and we also confirmed the presence of CA7-positive cells in human colon tissue, which prompted us to designate this as CA7 cluster, rather than BEST4 cluster. Given recent reports linking BEST4 to the pathophysiology of IBD[18] and colorectal cancer[23], conducting further research on the CA7 cluster using this ALI technique would be instrumental in advancing this area of study.

DCS cells were previously identified in mice to produce SC niche factors including EGF, DLL1, and DLL4 for supporting SC maintenance[11–13], but their existence in humans was not confirmed yet. We identified DCS-like cells differentially expressing DCS markers like REG4 and ARG2 in human IECs for the first time (Figure S2K). We also confirmed the non-exclusive expression of DLL1 and DLL4, but little of EGF, in the cluster (Figure S2L). Since our current understanding of this cluster is limited, additional analyses using this ALI technique will contribute to our future understanding of the functions of DCS-like cells.

The identification of the nc-GC population, recently characterized by the expression of both secretory-lineage and enterocyte markers[14], was another unexpected finding. Our UMAMP analyses suggest that while the GC and nc-GC populations cluster similarly, they possess distinct differences in their functions. Since the function of nc-GCs remains largely unknown, our monolayer culture is poised to make a significant contribution to clarifying their role.

While our ALI technique holds promise for further studies on human IECs, such

as 1) analyzing the interaction between human IECs and pathogens[7] or immune cells, and 2) exploring potential medications to control human IEC regeneration, it is essential to acknowledge certain limitations, including: 1) the inability to reproduce crypt-like folding structures, and 2) the experimental condition of direct exposure of cells to air, which differs from the actual physicochemical environment *in vivo*. We also need to consider the possibility that ALId7 cells may not have reached full differentiation when interpreting the scRNAseq results.

In conclusion, the newly developed monolayer culture system faithfully recapitulates the *in vivo* epithelial structure of the human colon in both homeostasis and regeneration. Its future applications hold promise for expanding our understanding of the human intestine in health and disease.

**Figure 1. Establishing *In Vitro* Culture of a Self-Organizing Human Colonic Epithelial Monolayer Using Air-Liquid Interface Culture Technique**

(A) Hematoxylin and Eosin (H&E) images of human colon monolayer cells at day 0, 4, 7, and 14 of ALI culture. Representative images of six rectum lines (n = 6). Scale bar: 50 μm.

(B) Cell height was quantified and plotted to compare ALId0 and ALId7. n = 4 rectum lines. Mean values ± SD are shown. Mann-Whitney U test: *p < 0.05.

(C) Sections of ALId7 monolayers stained for VIL1 (brush border marker), SLC26A3, MUC2, and CHGA. Representative images of three rectum lines (n =3). Scale bar: 50 μm.

(D) Transmission electron microscopy images showed the morphology of enterocytes (left panel), goblet cells (middle panel), and enteroendocrine cells (outlined with dashed line) with secretory granules (arrowhead) (right panel) at ALId7 or d14. Representative images of three rectum lines (n =3). Scale bar: 5 μm.

(E) The proliferation rate assessed by EdU positive cells per field in the human colon monolayer cells at ALI day 0, 1, 2, 4, and 7. n = 3 rectum lines. Mean values ± SD are shown. Ordinary one-way ANOVA with Tukey's multiple comparisons test: *p < 0.05; **p < 0.005; ***p < 0.0005.

(F) Heatmap analysis of major cell markers of SCs, TA cells, secretory progenitor cells, ECs, GCs, and EECs at various time points of ALI culture. n = 3 technical replicates per time point, except for n = 2 at ALI day 21.

(G) GSEA-based analysis of genes associated with the regenerative IECs in DSS-induced colitis in cells at ALI day 0 compared with those at ALI day 7. Normalized

enrichment scores (NES) and false discovery rates (FDR) are shown.

(H) GSEA-based analysis of the upregulated genes of colonic epithelium in UC patients compared with healthy donors (upper) and vice versa (lower), in cells at ALI day 0 compared with those at ALI day 7. NES and FDR are shown.

(I) Expression of LGR5, MKI67, AQP8, MUC2, and CHGA, defined by qPCR, in human colon monolayers at ALI day 0, 2, 4 and 7. Results were normalized to the day 0. Mean values ± SD were shown. n = 3 rectum lines/time point. Ordinary one-way ANOVA multiple comparisons: *$p < 0.05$; **$p < 0.005$; ***$p < 0.0005$; ****$p < 0.0001$.

**Figure 2. Transcriptomic Analysis of the Human IEC monolayer by Single-Cell Resolution Capturing Cellular Heterogeneity Resembling Homeostatic *in-Vivo* Mucosa**

(A-C) UMAP clustering (A), heatmap (B), and dot plot (C) of scRNAseq analysis of human colonic monolayer cells at ALI day 7 to represent top differentially expressed genes in each cluster, integrated out of three rectum lines (n = 3) derived from healthy donors.

(D) UMAPs of canonical SC markers (LGR5, OLFM4, ASCL2, SMOC2) derived from (A).

(E) *In situ* hybridization image of LGR5 RNA by RNAscope in the human colon monolayer cells at ALI day 7. A representative image of three rectum lines (n =3). Scale bar: 50 μm.

(F) Dot plot of canonical SC markers (LGR5, OLFM4, ASCL2, SMOC2) analyzed with (C).

(G) Bar graph of cell cycle analysis to represent proportion of cells in G1, G2M, or S phase.

(H-I) Pathway analysis to represent the top 6 upregulated pathways in the GC (H) and nc-GC (I) clusters. The top 150 differentially expressed genes in each cluster were used in this analysis.

(J) *In situ* hybridization image of CA7 RNA by RNAscope in the human colon monolayer cells at ALI day 7 (upper panel) and human colon surgical tissue (lower panel). Representative images of three rectum lines (n =3). Scale bar: 50 μm.

(K) Sub-clustering of the EEC cluster. UD (undifferentiated) represents cells expressing

no specific EEC subcluster markers. Stressed_Dying represents cells with higher mitochondrial gene ratio than the others (Figure S2J).

(L) Immunofluorescence of NEUROG3, 5HT, GLP-1, and SST in the human colon monolayer at ALI day 7. Representative images of three rectum lines (n =3). Scale bar: 50 μm.

## STAR+METHODS

## RESOURCE AVAILABILITY

### Lead Contact

Further information and requests for resources and reagents should be directed to and will be fulfilled by the lead contact, Thaddeus S. Stappenbeck (stappet@ccf.org).

### Material Availability

This study did not generate new unique reagents.

### Data and Code Availability

Bulk and single-cell RNAseq data have been deposited at GEO and are publicly available as of the date of publication. Accession numbers are listed in the key resources table.

## EXPERIMENTAL MODEL AND SUBJECT DETAILS

### Human Colonic Spheroid Lines

Human colonic crypts from healthy donors were obtained during routine endoscopy at the Washington University School of Medicine in collaboration with the Washington University Digestive Diseases Research Core Center (DDRCC) or at the Tokyo Medical and Dental University Hospital. This study was approved by the Washington University Institutional Review Board, Cleveland Clinic Institutional Review Board, and the Tokyo Medical and Dental University Scientific Ethics Committee. Written informed consent was obtained from all donors. The isolated crypts were collected and cultured as previously described[3]. In brief, to isolate crypt, biopsies were minced with fine scissors and digested in 1 mL of 2 mg/mL collagenase type I solution with 50 µg/mL gentamicin in washing media (DMEM/F12 supplemented with 1X L-glutamine, 1X penicillin/streptomycin and 10% FBS) for 20-30 min with pipetting every 5-10 min. Crypts were filtered through a 70-

μm strainer, incubated with 9 mL of ice-cold washing media and pelleted by centrifugation at 300 g for 5 min. Pelleted crypts were then suspended in 1 mL washing medium, transferred to a 1.5 mL tube and pelleted by centrifugation at 200 g for 5 min. The supernatant was carefully removed by pipette, and the pellet was re-suspended in Matrigel. The Matrigel mixture was plated into 24-well tissue culture plates on ice. Plates were flipped upside down and incubated at 37°C to polymerize the Matrigel and 500 μL of 50% L-WRN CM, a 50/50 mixture of L-WRN CM and fresh primary culture media (Advanced DMEM/F-12 supplemented with 20% fetal bovine serum, 1x L-glutamine or GlutaMax, 1x penicillin/streptomycin), supplemented with 10 μM Y-27632 and 10 μM SB 431542, was added to each well. Media was refreshed every 2-3 days. Grown spheroids were collected in Cell Recovery Solution, digested by TrypLE Express into small fragments, and passed every 3-4 days. These human colonic spheroid lines were maintained and passed up to 30 generations for the experiments in this paper.

**Human Tissue**

Formalin-fixed paraffin blocks of colonic surgical resection from non-IBD donors as healthy controls and UC patients were obtained from Department of Pathology and Immunology at the Washington University in St. Louis or Lerner Research Institute Biorepository Core at Cleveland Clinic. Five micro-meter sections from these blocks were stained for H&E, immunofluorescence, or RNAscope-based in situ hybridization.

## METHODS DETAILS

### ALI culture experiments

Grown human colonic spheroids were dissociated into single cells by TrypLE Express

digestion and seeded onto transwells pre-coated with 10% Matrigel diluted in PBS for 20min. 200,000 cells were seeded per well. Initially, 150 µL and 350 µL of 50% L-WRN media with 10uM Rock inhibitor (Y-27632) and TGF beta inhibitor (SB 431542) were added into the upper and lower chambers, respectively, to let the cells submerged in media for 5-7 days until they become confluent. Medium in the upper chamber was then removed to create an air-liquid interface. Cells were grown in ALI with 50% L-WRN medium (no Rock inhibitor or TGF beta inhibitor supplemented) in the bottom chamber for an additional 7-28 days to reach maturity with medium change every two or three days.

**Histology**

ALI cultured cells were fixed in 4% paraformaldehyde (PFA) for 30min at room temperature. The fixed cells were then dehydrated in 70% ethanol and were embedded in 2% agar followed by paraffin embedding, sectioning, and staining. Bright field histological images were acquired with an Olympus BX51 microscope. Cell height was quantified by averaging measurements from two slides per time point for each donor sample using the cellSens Imaging software.

**Immunostaining**

Slides were de-paraffinized and subjected to heat-induced antigen retrieval in Trilogy solution for 20min. Slides were blocked in PBS containing 2% BSA, 5% serum and 0.1% Triton-X for 1hr at room temperature, and then treated with primary antibodies at desired dilutions overnight at 4°C. They were then washed 3 times in PBS and incubated with secondary antibodies conjugated with desired fluorophores for 1 h at room temperature.

Fluorescent images were acquired with a Zeiss Axiovert 200M or a Zeiss Axio Observer 7 inverted microscope. ImageJ was used to uniformly adjust brightness and contrast. Information about primary antibodies and dilution used in the assay can be found in the key resources table and supplementary table S1, respectively.

**Transmission electron microscopy**

Cultures grown on transwell inserts were washed once in PBS, then fixed overnight at 4°C in 2.5% Glutaraldehyde + 4% Paraformaldehyde in 0.2M Sodium Cacodylate Buffer (pH 7.4). Fixative was removed and samples were stored in 0.2M Sodium Cacodylate Buffer at 4°C until further processing. Transwell membranes were removed from inserts, cut in half, then embedded in Eponate 12 Resin. Sections were cut with a Leica EM UC7 ultramicrotome. Semi-thin sections were transferred to glass microscope slides, stained with toluidine blue and imaged with an Olympus BX43 microscope equipped with a DP22 camera using 20x (NA), 40x (NA), and 63x (NA) objectives. Thin (200 nm) sections were stained with osmium tetraoxide and uranyl acetate, transferred to copper grids, and imaged using an FEI Tecnai G2 Spirit BioTWIN transmission electron microscope equipped with an 11 megapixel Orius 832 CCD camera. Operating voltages were held constant within imaging sessions.

**EdU incorporation assay**

ALI monolayer cells were treated with 10mM EdU for 3hrs and then fixed in 4% PFA for 30min at room temperature. EdU signal detection was performed according to the manufacturer's manual of the Click-iT EdU Cell Proliferation Kit or EdU Assay/EdU Staining Proliferation Kit. Samples were counterstained with Hoechst 33342, then whole mounted on glass microscope slides using Vectashield Vibrance mounting medium or

Vectashield mounting medium. Slides were imaged using a Zeiss Axio Observer 7 inverted microscope or an Olympus FV3000 confocal microscope. ImageJ was used to uniformly adjust brightness and contrast. Quantification was conducted by two blinded independent investigators.

**Quantitative PCR**

RNA was extracted from ALI cells using the RNeasy Micro Kit according to manufacturer's directions. Briefly, ALI cells were harvested in RLT buffer with 2-mercaptoethanol and stored in -80°C until use. RNA was extracted and eluted in 14ul of nuclease free water and stored at -80°C until use. RNA was quantified on Cytation 5 by diluting 1:1 with nuclease free water to determine the volume of RNA needed to convert to cDNA. cDNA was prepared using 1ug of starting RNA and using iScript reverse transcriptase kit according to manufacturer's directions. Quantitative PCR reaction was conducted with TB Green Advantage qPCR 2X- premix using a Bio-Rad CFX Connect Real-Time PCR Detection System. Primers were validated for specificity using a water control and conducting melt curve analysis. Data were analyzed using the Delta-Delta Ct method. Primer sequences for quantitative PCR used in this study are as follows; LGR5-forward: CCTTCATAAGAAAGATGCTGGAAT, LGR5-reverse: GTTTAATGGGGGAAATGTACAGAG; MKI67-forward: AAGAGAGTGTCTATCAGCCGAAGT, MKI67-reverse: GTGGCCTGTACTAAATTGACTGTG; AQP8-forward: GCCTGTCGGTCATTGAGAAT, AQP8-reverse: AGGGTTGAAGTGTCCACCAC; MUC2-forward: AGGATCTGAAGAAGTGTGTCACTG, MUC2-reverse: TAATGGAACAGATGTTGAAGTGCT; and CHGA-forward:

AGAATTTACTGAAGGAGCTCCAAG, CHGA-reverse: TCCTCTCTTTTCTCCATAACATCC.

**RNAscope based *in situ* hybridization**

ALI culture cells were fixed in 4% PFA for 30 min at room temperature and sequentially dehydrated in 10, 15 and 20% sucrose in PBS, and frozen in Tissue-Tek OCT compound. Five micron-thick cryosections were used for RNAscope based in situ hybridization according to protocols recommended by the manufacturer of RNAscope Multiplex Fluorescent Reagent Kit v2 (ACDBio). See the key resources table for details about probes used in the assays.

**Bulk RNA sequencing**

ALI cells were harvested as described for quantitative PCR. Total RNA quality was tested by Bioanalyzer. The RNA-Ribo-Zero method was employed for cDNA library construction. Sequencing datasets produced using an Illumina HiSeq3000 instrument were analyzed as follows. Reads were aligned to the reference human genome using STAR software (v2.7.8a). Gene counts were derived from uniquely aligned reads. To identify differentially expressed genes, DESeq2 package (v1.40.2) was used to calculate fold changes, p-values using a Wald test and adjusted using Benjamini-Hochberg correction. For pathway analysis, differentially expressed gene lists were analyzed by using g:Profiler through the gprofiler2 package (v0.2.2).

**Sample preparation for scRNAseq**

ALI transwells were washed by 1X DPBS-EDTA (0.05mM) once and incubated in TrypLE Express Enzyme at 37 °C for 25-30 mins, then pipetted 10 times with P1000 pipette and collected into a 15ml conical tube. Incubate the cell suspension at 37°C until the cells

mostly dissociate into singlets. The dissociated cell suspension was filtered through 20 μM strainer to purify cell singlets. Denovix CellDro FL automated cell counter was used to evaluate viability and singlet percentage of the prepared cell singlets. If necessary, the prepared cell singlets were sorted with BD FACS Melody Flow Cytometer by using Propidium Iodide and DRAQ5 double staining. Eventually, the prepared cell singlets from ALI (viability≥70%, singlet percentage≥70%) were immediately processed by following 10X Single Cell 3' Reagent Kits V3.1 Next GEM protocol (document # CG000204). Initially, 10,000 single cells were targeted using the Chromium Controller for cDNA synthesis and barcoding. Subsequent steps involved evaluating cDNA quality and quantity with a Bioanalyzer High Sensitivity DNA assay. The cDNA served as the foundation for fragmentation, end-repair, adapter ligation, and sample indexing. Bioanalyzer assays ensured proper library construction. Libraries were pooled, quantified using a Quantabio Q cycler, denatured, and sequenced on an Illumina Novaseq 6000 platform. The sequencing protocol comprised 28 cycles for the forward read and 91 cycles for the reverse read.

**scRNAseq data processing**

Sequence data were mapped onto the human genome (GRCh38) using CellRanger (v7.0.1) using default parameters. For downstream analysis, filtered gene-barcode matrices generated by CellRanger were read into the Seurat package (v5.0.0) on R (v4.3.0)/RStudio (v2023.09.1+494) (Butler et al., 2018; Cao et al., 2019; Trapnell et al., 2014). Plots generated from RStudio were adjusted with ggplot2 and processed with Adobe Illustrator CC. In Seurat, dead cells with high mitochondrial ratios (>20%) and potential doublets with high total transcript counts (>20,000) were first filtered out. The

resulting data were normalized using SCTransform with default parameters. The top 3,000 most variable features were calculated, and integration was performed to remove patient-to-patient variance for clustering. The first 40 PCs were used for graph-based clustering, which was visualized with UMAP-based dimensional reduction (Becht et al., 2018). Marker genes for each cluster were calculated using the wilcoxauc function from the presto package (v1.0.0). Visualization of gene expression was performed using various functions within the Seurat package, i.e. FeaturePlot, DoHeatmap, DotPlot, etc.

**ALI co-culture with *Shigella flexneri***

*Shigella flexneri* Castellani and Chalmers (M90T Sm) was cultured in TSB media to be its density at OD600 = approximately 1.0. the bacterial culture was pelleted at 3500G for 3 minutes and the bacterial palette was resuspended in 2 ml of advanced DMEM with 20 mM HEPES. 100 uL of the bacterial suspension was applied to ALId19 monolayer cells. Spin down the co-culture at 500G for 5 mins, then aspirate the bacterial suspension to restart ALI culture. After 24 hours of co-culture, the cells were fixed and processed for immunostaining.

**Key resources table**

| REAGENT or RESOURCE | SOURCE | IDENTIFIER |
|---|---|---|
| Antibodies | | |
| Rabbit monoclonal anti-Villin antibody (SP145) | Abcam | Cat#ab130751; RRID: AB_11159755 |
| Rabbit polyclonal anti-SLC26A3 antibody | Novus Biologicals | Cat#NBP1-84450; RRID: AB_11031898 |
| Mouse monoclonal anti-MUC2 antibody (F-2) | Santa Cruz Biotechnology | Cat#sc-515032; RRID: AB_2815005 |
| Rabbit polyclonal anti-Chromogranin A antibody | Abcam | Cat#ab15160; RRID: AB_301704 |
| Goat polyclonal anti-5-HT antibody | ImmunoStar | Cat#20079; RRID: AB_10719366 |
| Rabbit polyclonal anti-GLP-1 antibody | Bioss | Cat#BS-0038R; RRID: AB_10855332 |
| Rabbit polyclonal anti-Neurogenin 3 antibody | Bioss | Cat#BS-0922R; RRID: AB_10856983 |
| Rabbit polyclonal anti-SST antibody | Sigma-Aldrich | Cat#HPA019472; RRID: AB_1857360 |
| Mouse monoclonal anti-beta-Catenin antibody | BD Bioscience | Cat#610153; RRID: AB_397554 |
| Rabbit polyclonal anti-Shigella antibody | Abcam | Cat#ab65282; RRID: AB_1142846 |
| Alexa Fluor 488 donkey polyclonal anti-rabbit IgG (H+L) | Thermo Fisher Scientific | Cat#A-21206; RRID: AB_2535792 |
| Alexa Fluor 488 donkey polyclonal anti-mouse IgG (H+L) | Thermo Fisher Scientific | Cat#A-21202; RRID: AB_141607 |
| Alexa Fluor 488 donkey polyclonal anti-goat IgG (H+L) | Thermo Fisher Scientific | Cat#A-11055; RRID: AB_2534102 |
| Alexa Fluor 594 donkey polyclonal anti-rabbit IgG (H+L) | Thermo Fisher Scientific | Cat#A-21207; RRID: AB_141637 |
| Bacterial and virus strains | | |
| *Shigella flexneri* Castellani and Chalmers (M90T Sm) | ATCC | Cat#BAA-2402 |
| Biological samples | | |

| | | |
|---|---|---|
| Formalin-fixed paraffin blocks of colonic resection/biopsy samples derived from healthy donors | Washington University in St. Louis Department of Pathology & Immunology, Cleveland Clinic Lerner Research Institute Biorepository Core | N/A |
| Chemicals, peptides, and recombinant proteins | | |
| Advanced DMEM/F12 | Gibco | Cat#12634010 |
| DMEM/F12 | Sigma-Aldrich | Cat#D6421 |
| HEPES | Gibco | Cat#15630080 |
| Gentamicin solution | Sigma-Aldrich | Cat#G1272 |
| L-glutamine, 100X | Sigma-Aldrich | Cat#G7513 |
| GlutaMAX Supplement | Gibco | Cat#35050061 |
| Collagenase, Type I, powder | Gibco | Cat#17100017 |
| Fetal Bovine Serum | Sigma-Aldrich | Cat#F2442 |
| Matrigel | Corning | Cat# 354234 |
| Y-27632 dihydrochloride | R&D Systems | Cat#1254 |
| SB 431542 | R&D Systems | Cat#1614 |
| A83-01 | Tocris | Cat#2939 |
| Cell Recovery Solution | Corning | Cat#354253 |
| TrypLE Express Enzyme (1X), phenol red | Gibco | Cat#12605010 |
| Trilogy | Sigma-Aldrich | Cat#920P |
| Sodium Cacodylate Buffer, 0.2M, pH 7.4 | Electron Microscopy Sciences | Cat#11652 |
| Eponate 12 Resin | Pelco | Cat#18012 |
| Hoechst 33342 | Sigma-Aldrich | Cat#B2261 |
| Vectashield Vibrance mounting medium | Vector Laboratories | Cat#H-1700 |
| Vectashield mounting medium | Vector Laboratories | Cat#H-1000 |
| Tissue-Tek OCT compound | Sakura | Cat#4583 |
| Critical commercial assays | | |
| RNeasy Micro Kit | QIAGEN | Cat#74004 |
| NucleoSpin RNA, Mini kit for RNA purification | MACHEREY-NAGEL | Cat#740955 |
| iScript Reverse Transcription Supermix for RT-PCR | Bio-Rad | Cat#708841 |
| TB Green Advantage qPCR Premix | Takara | Cat#639676 |
| RNAscope Multiplex Fluorescent Reagent Kit v2 | ACDBio | Cat#323100 |
| RNAscope Probe- Hs-LGR5 | ACDBio | Cat#311021 |
| RNAscope Probe- Hs-CA7 | ACDBio | Cat#431961 |
| Click-iT EdU Cell Proliferation Kit for Imaging, Alexa Fluor 488 dye | Thermo Fisher Scientific | Cat# C10337 |
| EdU Assay / EdU Staining Proliferation Kit (iFluor 488) | Abcam | Cat#ab219801 |
| Deposited data | | |
| Raw data files for bulk RNA sequencing | This paper | GEO: |
| Raw data files for single-cell RNA sequencing | This paper | GEO: |

| Experimental models: Cell lines | | |
|---|---|---|
| L-WRN | ATCC | Cat#CRL-3276 |
| Oligonucleotides | | |
| qPCR primers, see also in Method Details | This paper | N/A |
| Software and algorithms | | |
| Enrichr | Ma'ayan Laboratory, Icahn School of Medicine at Mount Sinai, New York, NY; Chen et al., 2013; Kuleshov et al., 2016 | https://amp.pharm.mssm.edu/Enrichr/ |
| ImageJ | NIH | https://imagej.nih.gov/ij/ |
| cellSens Imaging Software | Olympus | Standard v3.2 |
| Graphpad Prism 9 | Graphpad | https://www.graphpad.com/scientificsoftware/prism/ |
| Other | | |
| Cytation 5 | BioTek | N/A |
| CFX Connect Real-Time PCR Detection System | Bio-Rad | N/A |

## ACKNOWLEDGEMENTS

This work was supported by the Crohn's & Colitis Foundation. We thank the Biorepository Core, Genomics Core, Flow Cytometry Core, and Imaging Core, Cleveland Clinic Lerner Research Institute, and the Genome Technology Access Center and Digestive Disease Research Core Center, Washington University in Saint Louis.

## AUTHOR CONTRIBUTIONS

T.S.S. conceptualized and supervised the study. S.F and Y.W. designed the study. S.F. performed and analyzed the data for most of the experiments. S. M. assisted with scRNAseq experiments. R.J.M performed the bioinformatics analysis. S.T.E., K.N., Y.H., S.S., and R.M. assisted with RNAscope and EdU assay. M.A.C, L.D.S, and R.O. provided scientific feedback. S.F. and T.S.S. wrote the manuscript. All authors contributed to the critical review of the manuscript.

## DECLARATION OF INTERESTS

T.S.S. is on the scientific advisory board for Janssen Pharmaceuticals and Amgen. T.S.S. is a founder of Mobius Care, Inc.

## REFERENCES


1. Miyoshi, H., Ajima, R., Luo, C.T., Yamaguchi, T.P., and Stappenbeck, T.S. (2012). Wnt5a Potentiates TGF-β Signaling to Promote Colonic Crypt Regeneration After Tissue Injury. Science *338*, 108–113. 10.1126/science.1223821.

2. Sato, T., Vries, R.G., Snippert, H.J., van de Wetering, M., Barker, N., Stange, D.E., van Es, J.H., Abo, A., Kujala, P., Peters, P.J., et al. (2009). Single Lgr5 stem cells build crypt-villus structures in vitro without a mesenchymal niche. Nature *459*, 262–265. 10.1038/nature07935.

3. VanDussen, K.L., Marinshaw, J.M., Shaikh, N., Miyoshi, H., Moon, C., Tarr, P.I., Ciorba, M.A., and Stappenbeck, T.S. (2015). Development of an enhanced human gastrointestinal epithelial culture system to facilitate patient-based assays. Gut *64*, 911–920. 10.1136/gutjnl-2013-306651.

4. Yui, S., Nakamura, T., Sato, T., Nemoto, Y., Mizutani, T., Zheng, X., Ichinose, S., Nagaishi, T., Okamoto, R., Tsuchiya, K., et al. (2012). Functional Engraftment of Colon Epithelium Expanded in Vitro from a Single Adult Lgr5+ Stem Cell. Nat. Med. *18*, 618–623. 10.1038/nm.2695.

5. Wang, Y., Chiang, I.-L., Ohara, T.E., Fujii, S., Cheng, J., Muegge, B.D., Ver Heul, A., Han, N.D., Lu, Q., Xiong, S., et al. (2019). Long-Term Culture Captures Injury-Repair Cycles of Colonic Stem Cells. Cell *179*, 1144-1159.e15. 10.1016/j.cell.2019.10.015.

6. Jenkins, D., Goodall, A., Drew, K., and Scott, B.B. (1988). What is colitis? Statistical approach to distinguishing clinically important inflammatory change in rectal biopsy

specimens. J. Clin. Pathol. *41*, 72–79. 10.1136/jcp.41.1.72.

7. Funkhouser-Jones, L.J., Xu, R., Wilke, G., Fu, Y., Shriefer, L.A., Makimaa, H., Rodgers, R., Kennedy, E.A., VanDussen, K.L., Stappenbeck, T.S., et al. (2023). Microbiota produced indole metabolites disrupt host cell mitochondrial energy production and inhibit Cryptosporidium parvum growth. BioRxiv Prepr. Serv. Biol., 2023.05.25.542157. 10.1101/2023.05.25.542157.

8. Yui, S., Azzolin, L., Maimets, M., Pedersen, M.T., Fordham, R.P., Hansen, S.L., Larsen, H.L., Guiu, J., Alves, M.R.P., Rundsten, C.F., et al. (2018). YAP/TAZ-Dependent Reprogramming of Colonic Epithelium Links ECM Remodeling to Tissue Regeneration. Cell Stem Cell *22*, 35-49.e7. 10.1016/j.stem.2017.11.001.

9. Wang, Y., Song, W., Wang, J., Wang, T., Xiong, X., Qi, Z., Fu, W., Yang, X., and Chen, Y.-G. (2019). Single-cell transcriptome analysis reveals differential nutrient absorption functions in human intestine. J. Exp. Med. *217*, e20191130. 10.1084/jem.20191130.

10. Ishikawa, K., Sugimoto, S., Oda, M., Fujii, M., Takahashi, S., Ohta, Y., Takano, A., Ishimaru, K., Matano, M., Yoshida, K., et al. (2022). Identification of Quiescent LGR5+ Stem Cells in the Human Colon. Gastroenterology *163*, 1391-1406.e24. 10.1053/j.gastro.2022.07.081.

11. Rothenberg, M.E., Nusse, Y., Kalisky, T., Lee, J.J., Dalerba, P., Scheeren, F., Lobo, N., Kulkarni, S., Sim, S., Qian, D., et al. (2012). Identification of a cKit+ Colonic Crypt Base Secretory Cell That Supports Lgr5+ Stem Cells in Mice. Gastroenterology *142*,

1195-1205.e6. 10.1053/j.gastro.2012.02.006.

12. Sasaki, N., Sachs, N., Wiebrands, K., Ellenbroek, S.I.J., Fumagalli, A., Lyubimova, A., Begthel, H., van den Born, M., van Es, J.H., Karthaus, W.R., et al. (2016). Reg4+ deep crypt secretory cells function as epithelial niche for Lgr5+ stem cells in colon. Proc. Natl. Acad. Sci. *113*, E5399–E5407. 10.1073/pnas.1607327113.

13. Schumacher, M.A., Liu, C.Y., Katada, K., Thai, M.H., Hsieh, J.J., Hansten, B.J., Waddell, A., Rosen, M.J., and Frey, M.R. (2023). Deep Crypt Secretory Cell Differentiation in the Colonic Epithelium Is Regulated by Sprouty2 and Interleukin 13. Cell. Mol. Gastroenterol. Hepatol. *15*, 971–984. 10.1016/j.jcmgh.2022.11.004.

14. Nyström, E.E.L., Martinez-Abad, B., Arike, L., Birchenough, G.M.H., Nonnecke, E.B., Castillo, P.A., Svensson, F., Bevins, C.L., Hansson, G.C., and Johansson, M.E.V. (2021). An intercrypt subpopulation of goblet cells is essential for colonic mucus barrier function. Science *372*, eabb1590. 10.1126/science.abb1590.

15. Bergstrom, K.S.B., and Xia, L. (2013). Mucin-type O-glycans and their roles in intestinal homeostasis. Glycobiology *23*, 1026–1037. 10.1093/glycob/cwt045.

16. Kiela, P.R., and Ghishan, F.K. (2016). Physiology of Intestinal Absorption and Secretion. Best Pract. Res. Clin. Gastroenterol. *30*, 145–159. 10.1016/j.bpg.2016.02.007.

17. Ito, G., Okamoto, R., Murano, T., Shimizu, H., Fujii, S., Nakata, T., Mizutani, T., Yui, S., Akiyama-Morio, J., Nemoto, Y., et al. (2013). Lineage-Specific Expression of

Bestrophin-2 and Bestrophin-4 in Human Intestinal Epithelial Cells. PLOS ONE *8*, e79693. 10.1371/journal.pone.0079693.

18. Parikh, K., Antanaviciute, A., Fawkner-Corbett, D., Jagielowicz, M., Aulicino, A., Lagerholm, C., Davis, S., Kinchen, J., Chen, H.H., Alham, N.K., et al. (2019). Colonic epithelial cell diversity in health and inflammatory bowel disease. Nature *567*, 49–55. 10.1038/s41586-019-0992-y.

19. Kanaya, T., Hase, K., Takahashi, D., Fukuda, S., Hoshino, K., Sasaki, I., Hemmi, H., Knoop, K.A., Kumar, N., Sato, M., et al. (2012). The Ets transcription factor Spi-B is essential for the differentiation of intestinal microfold cells. Nat. Immunol. *13*, 729–736. 10.1038/ni.2352.

20. Beumer, J., Puschhof, J., Bauzá-Martinez, J., Martínez-Silgado, A., Elmentaite, R., James, K.R., Ross, A., Hendriks, D., Artegiani, B., Busslinger, G.A., et al. (2020). High-Resolution mRNA and Secretome Atlas of Human Enteroendocrine Cells. Cell *181*, 1291-1306.e19. 10.1016/j.cell.2020.04.036.

21. Fujii, M., Matano, M., Toshimitsu, K., Takano, A., Mikami, Y., Nishikori, S., Sugimoto, S., and Sato, T. (2018). Human Intestinal Organoids Maintain Self-Renewal Capacity and Cellular Diversity in Niche-Inspired Culture Condition. Cell Stem Cell *23*, 787-793.e6. 10.1016/j.stem.2018.11.016.

22. Ohara, T.E., Colonna, M., and Stappenbeck, T.S. (2022). Adaptive differentiation promotes intestinal villus recovery. Dev. Cell *57*, 166-179.e6. 10.1016/j.devcel.2021.12.012.

23. He, X.-S., Ye, W.-L., Zhang, Y.-J., Yang, X.-Q., Liu, F., Wang, J.-R., Ding, X.-L., Yang, Y., Zhang, R.-N., Zhao, Y.-Y., et al. (2022). Oncogenic potential of BEST4 in colorectal cancer via activation of PI3K/Akt signaling. Oncogene *41*, 1166–1177. 10.1038/s41388-021-02160-2.

# Figure 1

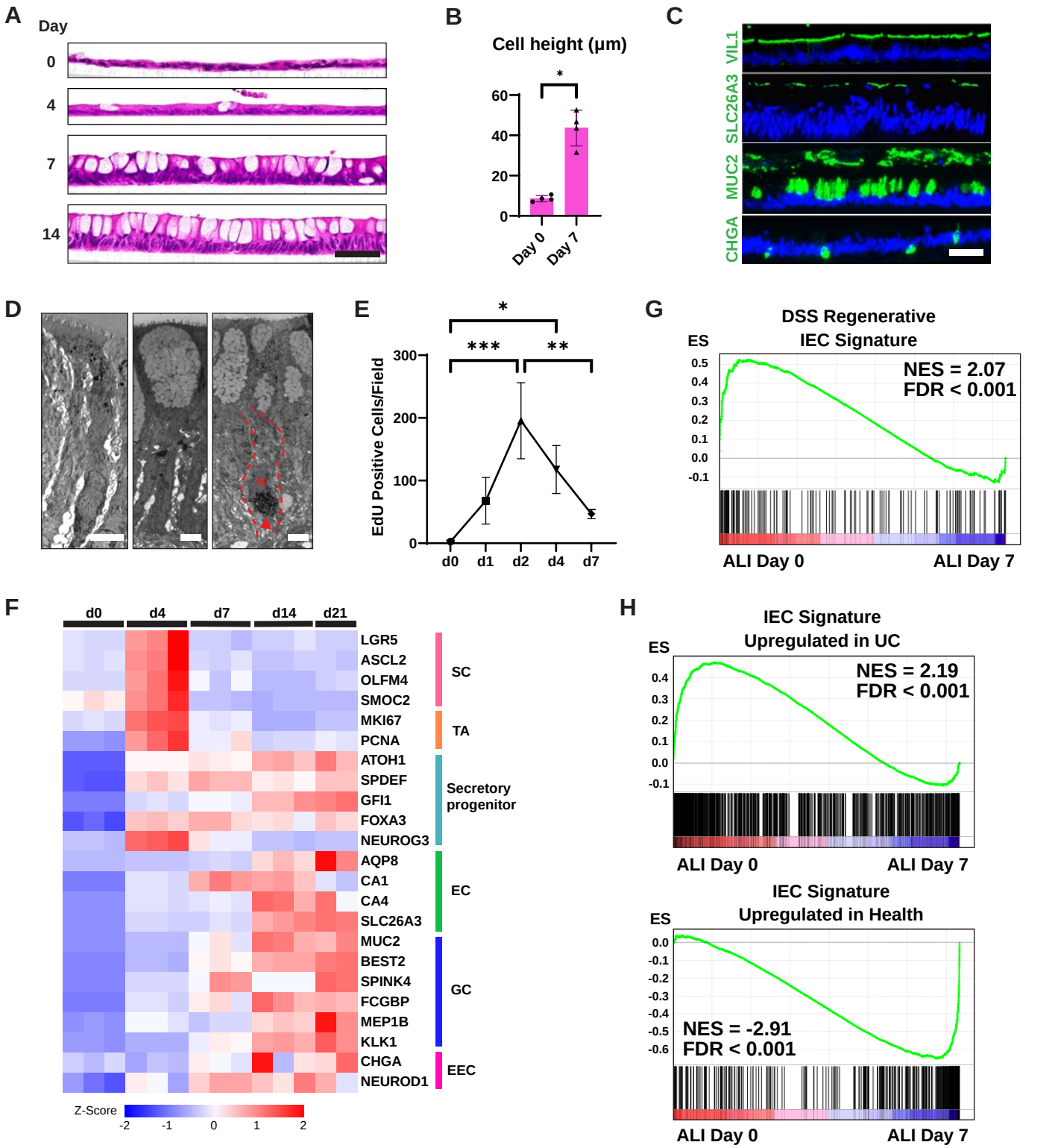
A
Day
0
4
7
14
B
Cell height (µm)
60
40
20
0
Day 0
Day 7
C
VIL1
SLC26A3
MUC2
CHGA
D
E
EdU Positive Cells/Field
300
200
100
0
d0
d1
d2
d4
d7
G
DSS Regenerative
IEC Signature
ES
NES = 2.07
FDR < 0.001
ALI Day 0
ALI Day 7
F
d0
d4
d7
d14
d21
LGR5
ASCL2
OLFM4
SMOC2
MKI67
PCNA
ATOH1
SPDEF
GFI1
FOXA3
NEUROG3
AQP8
CA1
CA4
SLC26A3
MUC2
BEST2
SPINK4
FCGBP
MEP1B
KLK1
CHGA
NEUROD1
SC
TA
Secretory
progenitor
EC
GC
EEC
Z-Score
-2
-1
0
1
2
H
IEC Signature
Upregulated in UC
ES
NES = 2.19
FDR < 0.001
ALI Day 0
ALI Day 7
IEC Signature
Upregulated in Health
ES
NES = -2.91
FDR < 0.001
ALI Day 0
ALI Day 7
I
LGR5
MKI67
AQP8
MUC2
CHGA
Relative expression
d0
d2
d4
d7

# Figure 2

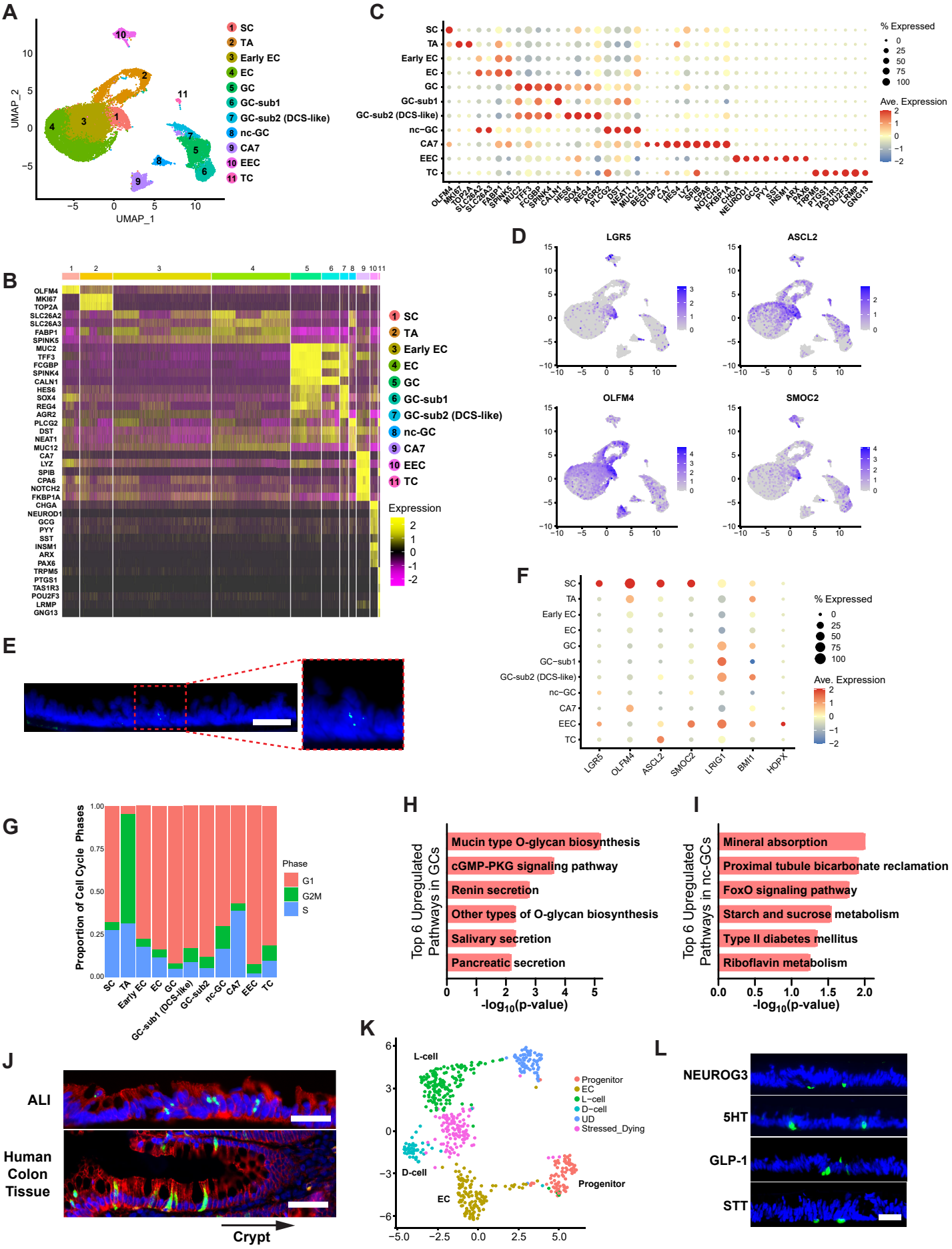
A
UMAP_1
UMAP_2
1 SC
2 TA
3 Early EC
4 EC
5 GC
6 GC-sub1
7 GC-sub2 (DCS-like)
8 nc-GC
9 CA7
10 EEC
11 TC
B
Expression
C
% Expressed
Ave. Expression
D
LGR5
ASCL2
OLFM4
SMOC2
E
F
G
Proportion of Cell Cycle Phases
Phase
G1
G2M
S
H
Top 6 Upregulated Pathways in GCs
Mucin type O-glycan biosynthesis
cGMP-PKG signaling pathway
Renin secretion
Other types of O-glycan biosynthesis
Salivary secretion
Pancreatic secretion
-log10(p-value)
I
Top 6 Upregulated Pathways in nc-GCs
Mineral absorption
Proximal tubule bicarbonate reclamation
FoxO signaling pathway
Starch and sucrose metabolism
Type II diabetes mellitus
Riboflavin metabolism
-log10(p-value)
J
ALI
Human Colon Tissue
Crypt
K
L-cell
D-cell
EC
Progenitor
Progenitor
EC
L-cell
D-cell
UD
Stressed_Dying
L
NEUROG3
5HT
GLP-1
STT

**Supplementary Figure 1**

(A) A representative H&E image of crypt abscess from disease mucosa of an ulcerative colitis case. ∗ indicates an abscess part which is surrounded by squamous-shaped IECs. Scale bar: 50 μm.

(B) H&E staining of human ileum cells at ALI day 14. A representative image of three rectum lines (n =3). Scale bar: 50 μm.

(C) MUC2 staining shows that goblet cells in the human colon monolayer in ALI culture produce extracellular mucus layers (outlined with red dashed lines) as *in vivo* structure. The extracellular mucus layers get thicker as ALI culture progresses.

(D) Immunofluorescence of *Shigella flexneri* (red) with beta Catenin (upper panel, green), and with MUC2 (lower panel, green), in homeostatic colon monolayer cells during ALI cultivation, co-cultured with *Shigella flexneri* applied to the apical side of the monolayer. Representative images of three independent experiments.

(E) Bright field imaging of human colon organoids three days after passage from ALI day 14 monolayer cells (upper panel, scale bar: 200 μm), and H&E staining of human colon monolayer cells at ALI day 14 after passage from ALI day 14 monolayer cells (lower panel, scale bar: 50 μm). Representative images of three rectum lines (n =3).

(F) Whole mount imaging of EdU staining in human colon monolayer cells at ALI day 0, 2, 4, and 7. Cells were stained for EdU (Green) and Nuclei (Gray). Representative images of three rectum lines (n =3).

(G-H) GSEA-based analysis of genes associated with fetal-like IECs (G), and with YAP signaling (H), in cells at ALI day 0 compared with those at ALI day 7. NES and FDR are shown.

(I-J) Heatmap of selected major YAP target genes (I), and WNT target genes (J), of human colon monolayer cells at ALI day 0, 2, 7, 14, and 21. n = 3 technical replicates per time point, except for n = 2 at ALI day 21.

**Supplementary Figure 2**

(A) UMAP clustering of scRNAseq analysis of human colonic spheroids cultured in WRN-CM for three days, integrated out of the same three rectum lines (n = 3) as used in scRNAseq analysis at ALI day 7.

(B) UMAPs of HOPX (colitis-associated regenerative SC marker defined in mice), LRIG1 (quiescent SC marker defined in mice), BMI1 (reserve SC marker defined in mice), associated with Figure 2D.

(C) UMAPs of MKI67 and PCNA. Seeing this along with S2D, most of PCNA positive cells are in S phase, while most of MKI67 positive cells are in G2M phase.

(D) Cell cycle analysis to visualize cells in G1, G2M, or S phase in UMAPs, associated with Figure 2G.

(E) UMAP of mitochondrial gene ratio represents the GC-sub1 cluster with higher mitochondrial gene ratio than the other GC clusters.

(F) UMAP of PLCG2, a candidate marker of nc-GC cells.

(G-H) UMAPs of BEST4 and CA7 (G), SPIB and GP2 (H), associated with CA7 cluster.

(I) Dot plot of ECC subcluster marker expression in each EEC subcluster, associated with Figure 2K.

(J) UMAP of mitochondrial gene ratio in ECC subclusters.

(K-L) UMAPs of REG4 and AGR2 (K), DLL1, DLL4, and EGF (L), associated with DCS-like cluster.

# Supplementary Figure 1

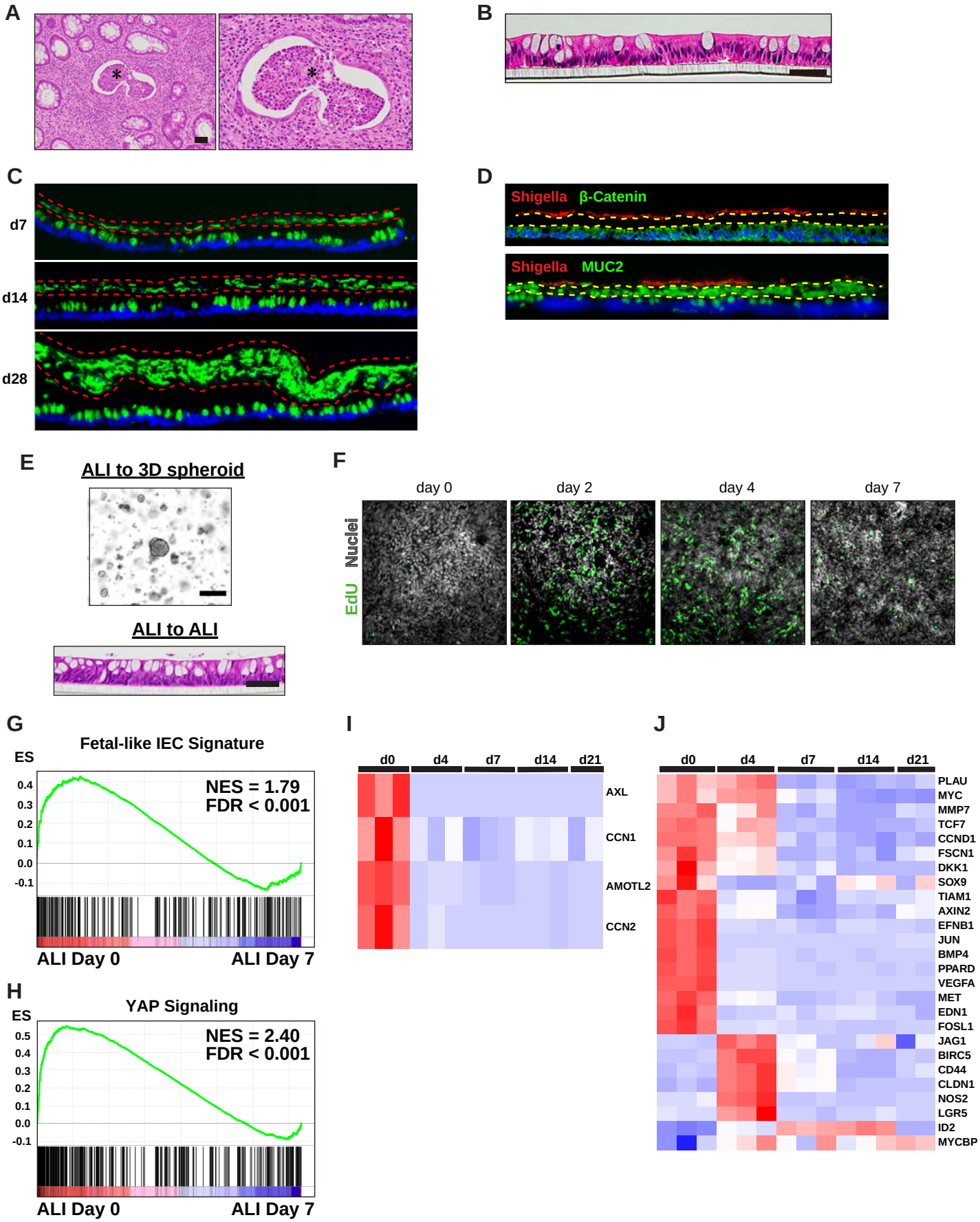

# Supplementary Figure 2

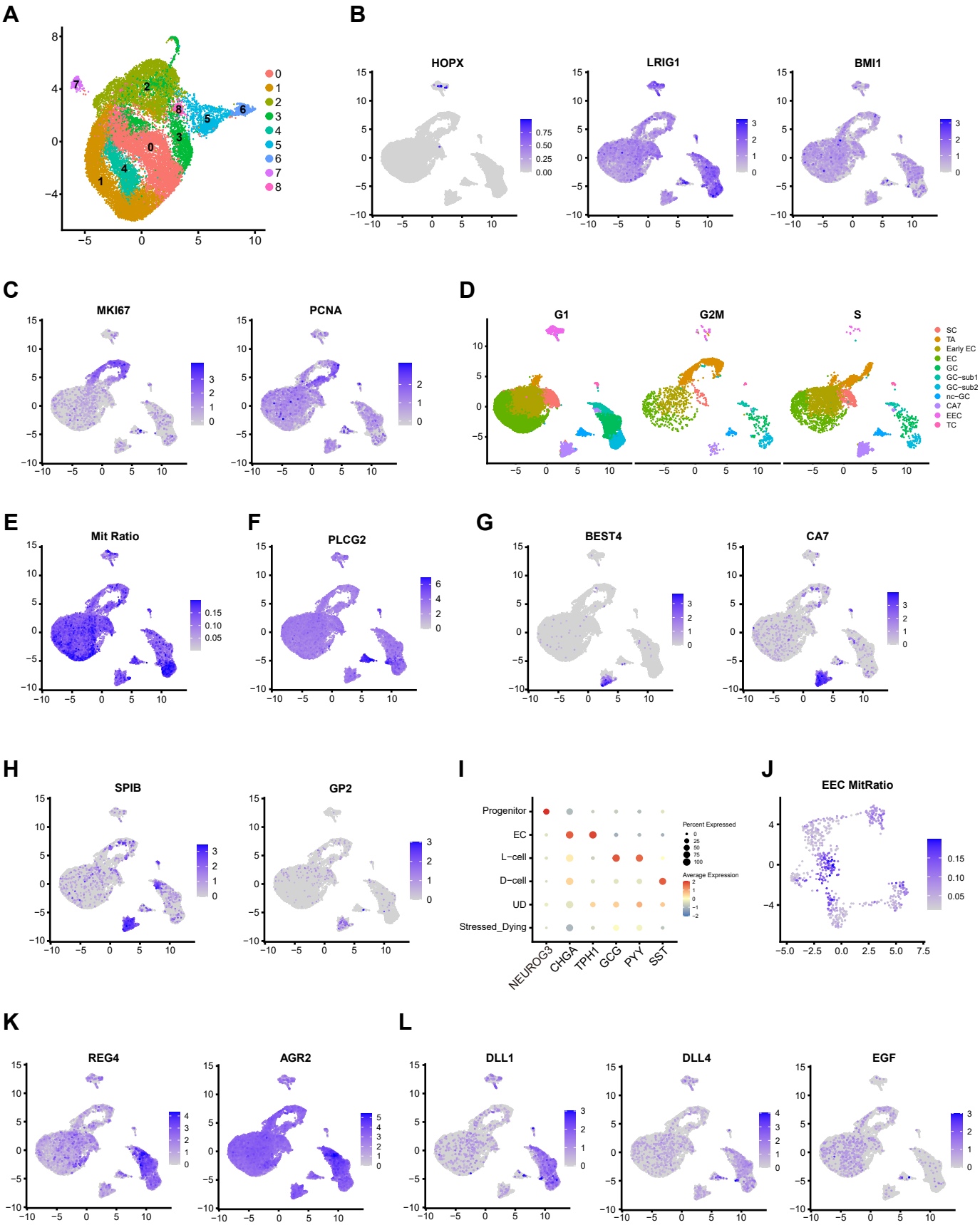

**Supplementary Table S1**

| Antibody | Dilution |
|---|---|
| Rabbit monoclonal anti-Villin antibody (SP145) | 1/1000 |
| Rabbit polyclonal anti-SLC26A3 antibody | 1/100 |
| Mouse monoclonal anti-MUC2 antibody (F-2) | 1/100 |
| Rabbit polyclonal anti-Chromogranin A antibody | 1/2000 |
| Goat polyclonal anti-5-HT antibody | 1/5000 |
| Rabbit polyclonal anti-GLP-1 antibody | 1/200 |
| Rabbit polyclonal anti-Neurogenin 3 antibody | 1/200 |
| Rabbit polyclonal anti-SST antibody | 1/1000 |
| Mouse monoclonal anti-beta-Catenin antibody | 1/1000 |
| Rabbit polyclonal anti-Shigella antibody | 1/1000 |